Calibration of the 7—Equation Transition Model for High Reynolds Flows at Low Mach

2016 J. Phys.: Conf. Ser. 753 082027

(http://iopscience.iop.org/1742-6596/753/8/082027)

Calibration of the $\gamma-$Equation Transition Model for High Reynolds Flows at Low Mach

S Colonia, V Leble, R Steijl and G Barakos.
School of Engineering, University of Glasgow, Glasgow G12 8QQ, Scotland
E-mail: Simone.Colonia@glasgow.ac.uk, George.Barakos@glasgow.ac.uk

Abstract. The numerical simulation of flows over large-scale wind turbine blades without considering the transition from laminar to fully turbulent flow may result in incorrect estimates of the blade loads and performance. Thanks to its relative simplicity and promising results, the Local-Correlation based Transition Modelling concept represents a valid way to include transitional effects into practical CFD simulations. However, the model involves coefficients that need tuning. In this paper, the $\gamma-$equation transition model is assessed and calibrated, for a wide range of Reynolds numbers at low Mach, as needed for wind turbine applications. An aerofoil is used to evaluate the original model and calibrate it; while a large scale wind turbine blade is employed to show that the calibrated model can lead to reliable solutions for complex three-dimensional flows. The calibrated model shows promising results for both two-dimensional and three-dimensional flows, even if cross-flow instabilities are neglected.

Nomenclature

C	Chord	S_{ij}	Strain-rate tensor, $0.5\left(\frac{\partial u_i}{\partial x_j}+\frac{\partial u_j}{\partial x_i}\right)$
Cd	Drag coefficient	Tu	Turbulence intensity, $100\sqrt{2k/3}/U$
C_f	Skin friction coefficient	Tu_L	Local turbulence intensity
Cl	Lift coefficient	u_i	Velocity component in the i-direction
Cl_α	Lift coefficient slope	U_W	Wind speed
H	Boundary layer shape factor	U_0	Local freestream velocity
k	Turbulent kinetic energy	$\mathbf{W}$	Vector of conservative variables
Ma	Mach number	x_i	Spatial coordinate in the i-direction
$\mathbf{P}$	Vector of primitive variables	X_{tr}	Transition position
$\mathbf{R}$	Vector of residuals	y	Nearest wall distance
R	Blade radius	$\alpha_{Cl=0}$	Zero lift angle
Re	Reynolds number	γ	Intermittency
Re_θ	Momentum-thickness Re, $\rho U_0\theta/\mu$	$\lambda_{\theta L}$	Local pressure gradient parameter
Re_{θ_c}	Critical Momentum-thickness Re	μ_t	Eddy viscosity
Re_v	Strain-rate (or vorticity) Re, $\rho Sy^2/\mu$	μ	Molecular viscosity
S	Strain-rate absolute value, $(2S_{ij}S_{ij})^{1/2}$	ω	Turbulence dissipation rate

1. Introduction

In many engineering applications, flow computations without considering the transition from laminar to fully turbulent flow may result in incorrect predictions. Thus, the significance of the transition process in various aerodynamics applications can not be understated, and proper prediction of boundary layer transition is vital in aerodynamic design. Nevertheless, methods for simulating transitional flows are still not frequently used in computational fluid dynamics.

The main types of transition are natural and bypass. Natural transition occurs at low free-stream turbulence intensity (Tu), usually less than 1%. In the initial stage, known as receptivity, environmental disturbances, such as free-stream noise and turbulence and surface roughness, propagate as small perturbations within the boundary layer. For 2D flows, these instabilities take the form of periodic waves, known as Tollmien-Schlichting (TS) waves, which, when the momentum-thickness Reynolds number (Re_θ) exceeds a critical threshold, are gradually amplified in the laminar boundary layer. Their evolution is well captured by the linear stability theory; however, as these instabilities grow, they begin to exhibit non-linear interactions leading rapidly to the breakdown to turbulence. In 3D boundary layers, the mean velocity profile also displays a cross-flow (CF) component other than the stream-wise. The stream-wise velocity profile generates waves similar to the TS waves observed in 2D flow, while the cross-flow velocity profile induces CF waves that propagate in a direction normal to the free-stream. Although the same linear stability theory is applicable to both wave types, the non-linear interactions are different for TS and CF instabilities [1] . In various situations, laminar to turbulent transition occurs at Reynolds numbers lower than what predicted by the linear stability theory, this suggests that another transition mechanism exists. Indeed, if the laminar boundary layer is exposed to large free-stream turbulence levels, larger than 1%, bypass transition process occurs. The term bypass means that the natural transition mechanism driven by the TS or CF waves has been short-circuited and the disturbances are amplified by non-linear phenomena.

At present, the most popular methods for predicting transition are the ones based on the linear stability theory such as the e^N model developed more than half a century ago by Smith and Gamberoni [2] and by van Ingen [3] . This approach uses the linear stability theory to calculate the growth of the disturbance amplitude in the boundary layer. The so-called N factor represents the total growth rate of the most unstable among the disturbances and it is not universal. The e^N method has been successfully used to predict transition for a wide range of test cases. However, although there are examples of full 3D implementations of the e^N method [4, 5] ,the main obstacle to its use with the current Computational Fluid Dynamics (CFD) methods lies in the complex infrastructure required to apply the model and the development of simpler methods is of pratical interest. Furthermore, the linear stability theory can not be employed to predict bypass transition.

An alternative to this approach is to use the concept of intermittency, γ, which represents the fraction of time that the flow is turbulent during the transition phase. The intermittency is zero in the laminar region and becomes one in the fully turbulent region, thus can be used to control the onset and the development of transition. From experimental observations, the development of intermittency is almost general for the steady boundary layer on a flat plate, therefore the onset location can be correlated. Most correlations usually relate the transition momentum thickness Reynolds number to turbulence intensity and the pressure gradient. Among them, the most commonly used are the correlation of Abu-Ghannam and Shaw [6] , Michel's criterion [7] and the Cebeci and Smith approach [8] .

The Local-Correlation based Transition Modelling (LCTM) concept was proposed by Menter et. al. [9] almost a decade ago and fully disclosed later in [10] . The first formulation of the LCTM, termed γ-Re$_\theta$ model, involves two additional transport equations, for the turbulence intermittency and for the transition onset correlation respectively, which allow combining experimental correlations in a local fashion with the underlying turbulence model.

A strong characteristic of the LCTM concept is its flexibility and relatively straightforward implementation into practical CFD simulations allowing the inclusion of different transitional effects for which enough experimental data is available to tune and optimise the model. Since its introduction, the correlation based transition model has shown promising results and various works have been done to improve it. Recently, a simplified version of the model has been presented [11] with the goal to maintain the LCTM concept, including the ability to model various transitional processes, reduce the formulation to only the γ-equation providing tunable coefficients to match the required application, and obtain a Galilean invariant formulation. In [11] , Menter et al. assessed the model for different test cases covering a range of Reynolds numbers between 50×10^3 and 500×10^3 at subsonic and transonic Mach numbers. Thus, further works are needed to evaluate the γ-equation model at more extreme conditions such as high Reynolds numbers (i.e. $Re \geq 1 \times 10^6$), very low Reynolds numbers (i.e. $Re \leq 50 \times 10^3$) and supersonic/hypersonic flows.

In this paper, the $\gamma-$equation transition model is calibrated for all Reynolds numbers flows at low Mach numbers to be employed for wind turbine applications, allowing for better estimates of flow transition. For wind turbine applications, flow analysis and design methods based on the RANS equations have been extensively employed by several research groups [12] . The most common approach is to use fully turbulent simulations ignoring the transition process. However, fully turbulent flow solutions have been shown to over-predict the aerodynamic drag impacting the design of wind turbine aerofoils [13, 14, 15] . Brodeur and van Dam [13] demonstrated the validity of the e^N method for two-dimensional flows around wind turbine profiles. As mentioned before, the complex infrastructure required by the methods affect it applicability to complex three-dimensional cases.

In the context of the present work, the $\gamma-$equation transition model of Menter has been implemented in the CFD code of the University of Glasgow, HMB3 [16, 17] . In section 2 the main features as well as the tunable constants of the model are discussed. Then, section 3 contains a summary of the selected test cases while in section 4 the calibration approach and the results are presented. The goal was not to obtain perfect agreement with linear stability results, since this would require to change the model correlation with more complex ones, but to tolerate some differences as part of the approach taken to formulate the original model [11] . Finally, in section 5 conclusions of the present work are given as well as suggestions for future improvements.

2. The $\gamma-$Equation Transition Model

The Helicopter Multi-Block (HMB3) code [17] , developed at Glasgow University, has been used in the present work. For the complete definition of the $\gamma-$equation LCTM the reader is referred to the original work of Menter et al. [11] whose notation is preserved in the present paper. A first set of parameters is the one used in the critical momentum-thickness Reynolds number correlation

$$Re_{\theta_c}\left(Tu_L, \lambda_{\theta L}\right) = C_{TU1} + C_{TU2} \exp\left(-C_{TU1} Tu_L F_{PG}\left(\lambda_{\theta L}\right)\right) \tag{1}$$

and define the minimum (C_{TU1}), maximum ($C_{TU1}+C_{TU2}$) and the rate of decay with an increase of the turbulence intensity (C_{TU3}) of the critical Re_{θ_c} number. A further set of constants is introduced in the function employed to include in the transition onset the effect of the streamwise pressure gradient

$$F_{PG}\left(\lambda_{\theta L}\right) = \begin{cases} min\left(1 + C_{PG1}\lambda_{\theta L}, C_{PG2}^{lim}\right) & \lambda_{\theta L} \geq 0 \\ \\ min\left(1 + C_{PG2}\lambda_{\theta L}, C_{PG2}^{lim}\right) & \lambda_{\theta L} < 0 \end{cases} \tag{2}$$

Here, C_{PG1} controls the value of Re_{θ_c} in areas with favourable pressure while C_{PG2} with adverse pressure gradient. In [11] an additional constant C_{PG3} is considered to correct Re_{θ_c} in regions with separation if necessary but it is set to zero and here the same approach is followed.
The authors believe that a further tunable parameter, here named C_{onset1}, can be identified in the function that controls the transition onset as follow

$$F_{onset1} = \frac{Re_v}{C_{onset1} Re_{\theta_c}} \quad \text{with} \quad C_{onset1} = 2.2. \tag{3}$$

Since the triggering of the transition is based on Re_v instead of Re_θ computed from the velocity profile, C_{onset1} should change accordingly with the ratio between these two Reynolds numbers. This ratio can be expressed as function of the shape factor, H, or the pressure gradient parameter λ_θ. In the original model the value 2.2 is selected to achieve a F_{onset1} equal to one within a Blasius boundary layer and this effect is taken into account through the correlation for the critical momentum-thickness Reynolds number presented in equation (1). However, previous works [10, 15] for the γ-Re_θ model observed the necessity to re-scale C_{onset1} at high Reynolds numbers.
For the results shown in the present work, the model has been coupled with the $k-\omega$ SST turbulence model of Menter [18] and the Kato-Launder formulation [19] of the production term is employed. To eliminate the non-physical decay of turbulence variables in the freestream for external aerodynamic problems, the additional sustaining terms to the equations of the SST model have been employed [20] .

3. Description of Test Cases

For the calibration of the model and its assessment, with particular focus on wind turbine applications, an aerofoil and a wind turbine blade have been used. The aerofoil computations are performed at Mach numbers typical of wind turbine applications, i.e. $Ma \approx 0.1$. Three different operative conditions, summarised in table 1, are considered for the wind turbine blade. The aerofoil selected is the DU00-w-212, an aerofoil currently employed in the AVATAR project for large scale wind turbines [21] . The computational domain can be seen in figure 1a. The domain is divided in 70 blocks and 82 thousands cells with 331 cells around the aerofoil, 155 cells in the normal direction and 103 cells from the TE to the far-field. The employed normal spacing in terms of the chord, c, at the wall is $1 \times 10^{-6}c$, while spacings of $1 \times 10^{-3}c$ and $1 \times 10^{-4}c$ are used around the aerofoil at the leading (LE) and trailing (TE) edges, respectively. The far-field is placed at a distance $40c$, where c is the aerofoil chord.
The AVATAR wind turbine blade [21] is selected as 3D case. Figure 1b shows a sketch of the blade and a section cut. The grid consists of 15 millions cells with 325 points around the section, 295 in the span-wise direction and 101 in the normal direction. The number of blocks in which the domain is decomposed is 442 and the spacing at the wall is $5 \times 10^{-7}c_{max}$. In this case the far-field is placed at 6 blade radius towards the outflow and 3 blade radius towards the inflow and in the radial direction. Previous works [22, 23] have shown that, with the boundary condition implementation in the HMB3 code, the chosen distances for the far-field do not affect the solution and similar settings have been successfully employed to simulate the NREL Annex XX [23] and MEXICO [24, 25] experiments.
In all considered geometries, hyperbolic laws are employed for the cells distributions along all the blocks' edges and steady-state simulations have been performed.

4. Assessment and Calibration of the $\gamma-$equation Model

4.1. 2-D Cases

In the present work, only natural transition, i.e. $Tu < 1\%$, is considered at high Reynolds numbers and cross-flow instabilities are neglected. The first proposed modification to the model

Wind speed, U_W (m/s)	RMP	Pitch
10.00	8.6	0.00°
10.50	9.0	0.00°
12.00	9.6	3.98°

Table 1: Summary of the selected operative conditions for the AVATAR wind turbine blade (RPM: rotations per minute).

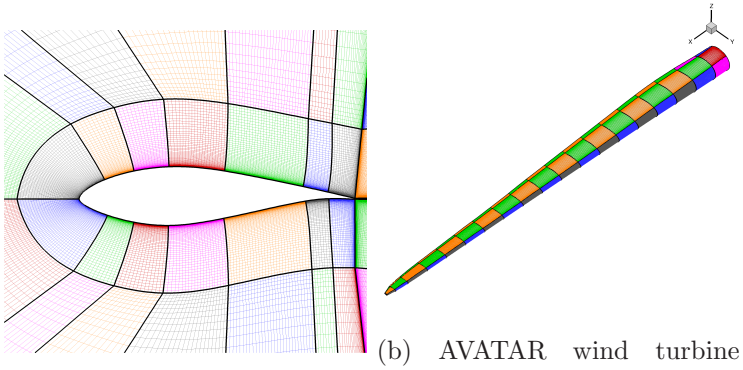

(a) DU00-w-212 aerofoil. (b) AVATAR wind turbine blade.

Figure 1: CFD grids.

constants is a rescaling of C_{TU1} and C_{TU2} in equation (2) from 100.0 and 1000.0 to 163.0 and 1002.25, respectively. The choice of this constants is done so that equation (1) exactly matches the Abu-Ghannam and Shaw correlation [6] for zero pressure gradient, i.e. $\lambda_{\theta L} = 0$. Furthermore, the minimum value of 163.0 for the critical momentum-thickness Reynolds number, Re_{θ_c}, is in accordance with the Tollmien-Schlichting limit of stability [6] .

For the flow around the DU00-w-212 aerofoil at high Reynolds numbers simulations performed with Xfoil [26] are employed here as benchmark for the calibration of the LCTM. Xfoil is a well known tool for 2D aerofoil computations, firstly developed at the Massachusetts Institute of Technology in the 1980s and since then widely used by companies and research institutes. The reason behind the choice of this tool is that it employs the e^N method to predict the transition position.

Figures 2a-c show the skin friction coefficient on the lower and upper surfaces of the aerofoil, as functions of the position along the chord, for different high Reynolds numbers at low free-stream turbulence intensity $Tu = 0.0816\%$. The results of the original model are in reasonable agreement with Xfoil predictions only at $Re = 3 \times 10^6$ as shown in figure 2a. When the Reynolds further increases, the original model predicts too early transition as can be observed in figures 2b-g. The first proposed modification improved the agreement of the model with Xfoil predictions at $Re = 3 \times 10^6$; however, it was not enough at higher Reynolds numbers.

As mentioned in section 2, previous works in the literature for the γ-Re$_\theta$ model have observed that the constant employed in the ratio defined in equation 3 needs to be increased [10, 15] . Thus, a gradual increase of the constant C_{Onset1} to 2.75, 3.3, 3.85 and 4.4 has been considered here. In figures 3a-c skin friction predictions are provided for different values of C_{Onset1}. The results show that an optimal range of C_{Onset1}, which leads to a good agreement with Xfoil's e^N results, can be found at each Reynolds number.

In figure 4 the optimal values of C_{Onset1}, among the ones employed, are reported for the considered Reynolds numbers, while a summary of all the modified constants can be found

in table 2. Looking at figure 4, it is possible to notice that a simple logarithmic curve fitting, reported in table 2, can be used to define C_{Onset1} as a function of the Reynolds number for $1 \times 10^6 \leq Re \geq 15 \times 10^6$. In the original model [11] , Menter et al. observed that the ratio $Re_v/(2.2Re_\theta)$ can change by as much as a factor of around 2.2 for typical values of the boundary layer shape factor. For this reason a maximum value of 4.84 is employed here for C_{Onset1}, while the minimum value of 2.2 is used to recover the transition onset of the original model for $Re < 3 \times 10^6$. Figures 5a-c show predictions of the skin friction coefficient on the lower and upper surfaces of the DU00-w-212 aerofoil for different Reynolds numbers when the fitting curve is employed. The results are in very good agreement with the predictions obtained using the e^N method for all the Reynolds numbers considered.

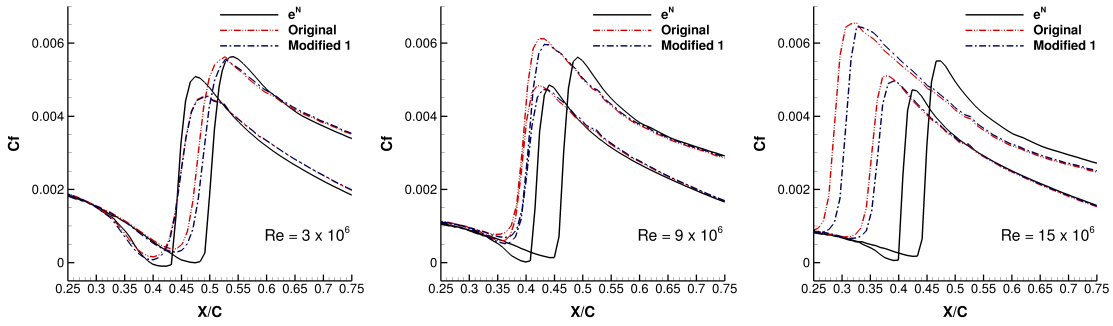

(a) $Re = 3 \times 10^6$. (b) $Re = 9 \times 10^6$. (c) $Re = 15 \times 10^6$.

Figure 2: Skin friction coefficient, C_f, at various Reynolds numbers: effect of the proposed $C_{TU1} = 163.0$ and $C_{TU2} = 1002.25$ on the predicted transition region. DU00-w-212 aerofoil at $Ma = 0.1$ and free-stream $Tu = 0.0816\%$ and $\mu_t/\mu = 1.0$.

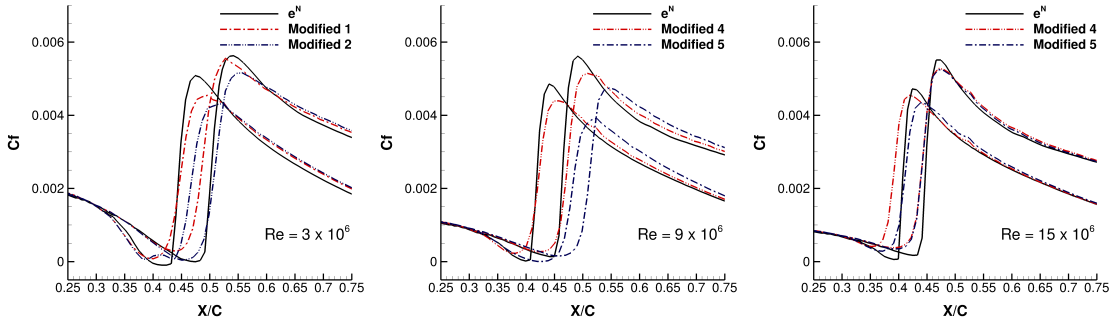

(a) $Re = 3 \times 10^6$. (b) $Re = 9 \times 10^6$. (c) $Re = 15 \times 10^6$.

Figure 3: Skin friction coefficient, C_f, at various Reynolds numbers: effect of C_{Onset1} on the predicted transition region. DU00-w-212 aerofoil at $Ma = 0.1$ and free-stream $Tu = 0.0816\%$ and $\mu_t/\mu = 1.0$.

When employed to predict lift and drag coefficients at various angles of attack, the $\gamma-$equation LCTM with the logarithm curve fitting for the transition onset, shows good agreement with Xfoil computations and the experiments conducted at the DNW-HDG wind tunnel in Göttingen (Germany) by ECN [27] and CENER [28] in the context of the AVATAR project. The results can be seen from figures 6a-b for $Re = 3 \times 10^6$ and figures 7a-b for $Re = 15 \times 10^6$. As expected, the original model predicts an earlier transition and thus a much higher drag coefficient, in particular

Model	C_{TU1}	C_{TU2}	C_{onset1}
Original	100.00	1000.00	2.20
Modified 1	163.00	1002.25	2.20
Modified 2	163.00	1002.25	2.75
Modified 3	163.00	1002.25	3.30
Modified 4	163.00	1002.25	3.85
Modified 5	163.00	1002.25	4.40
Log. Fit.	163.00	1002.25	$min(4.84, max(2.2, 1.388ln(Re \times 10^{-6}) + 0.705))$

Table 2: Summary of the employed constants.

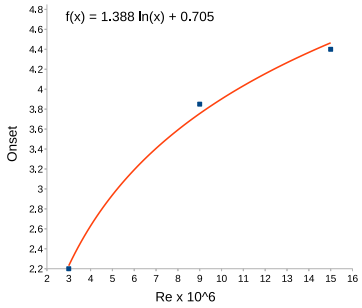

Figure 4: Proposed curve fitting for C_{onset1} at $3 \times 10^6 \leq Re \leq 15 \times 10^6$.

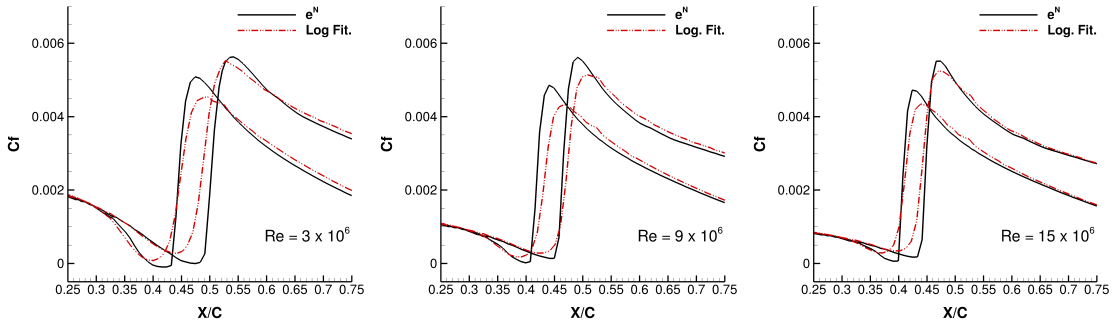

(a) $Re = 3 \times 10^6$. (b) $Re = 9 \times 10^6$. (c) $Re = 15 \times 10^6$.

Figure 5: Skin friction coefficient, C_f, at various Reynolds numbers: effect of the proposed logarithm curve fitting on the predicted transition region. DU00-w-212 aerofoil at $Ma = 0.1$ and free-stream $Tu = 0.0816\%$ and $\mu_t/\mu = 10.0$.

at low angles of attack, for the two higher Reynolds numbers considered, while the proposed calibrated model shows better agreement with Xfoil and experimental data capturing the low drug bucket. At the highest Reynolds number considered, 15×10^6, the original model does not even predict a low drug bucket while employing the logarithm curve fitting for the transition onset, more reliable results are obtained as can be seen in figure 7b. Furthermore, the results shown in figures 6c and 7c indicate that even though the calibration was perfomed on the fine grid, mesh convergence was obtained and the results did not change when further refinement has been considered. The medium and coarse grids have been defined from the fine grid by removing every other point in each direction one and two times, respectively, while the finer mesh has been obtained increasing the number of points by a factor $\sqrt{2}$ in both directions. In

all grids y^+ was varied accordingly. Tables 3 and 4 summarise some important design properties computed for the DU00-w-212 aerofoil such as the low drag bucket extension, the zero lift angle ($\alpha_{Cl=0}$) and the lift slope (Cl_α). Note that Cl_α is computed here using the lift coefficients at $-4°$ and $4°$ angles of attack. In comparison with Xfoil results; the low drag bucket extension as well as the zero lift angle are correctly predicted, less than 1% difference, by the calibrated model for all cases considered, while the original transitional model leads to reliable results only for $Re = 3 \times 10^6$. Regarding the Cl_α, slightly lower, around 3%, values are predicted by both models.

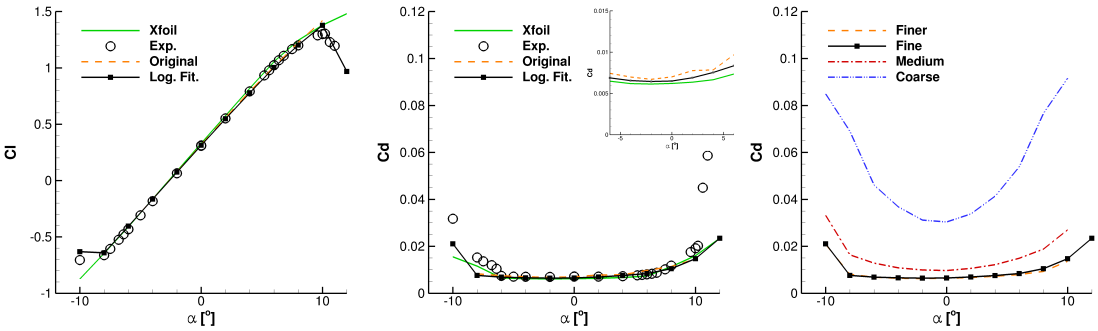

(a) Cl vs α. (b) Cd vs α. (c) Cd vs α.

Figure 6: Polars for DU00-w-212 aerofoil at $Re = 3 \times 10^6$, $Ma = 0.075$ and free-stream $Tu = 0.0864\%$ and $\mu_t/\mu = 0.05$.

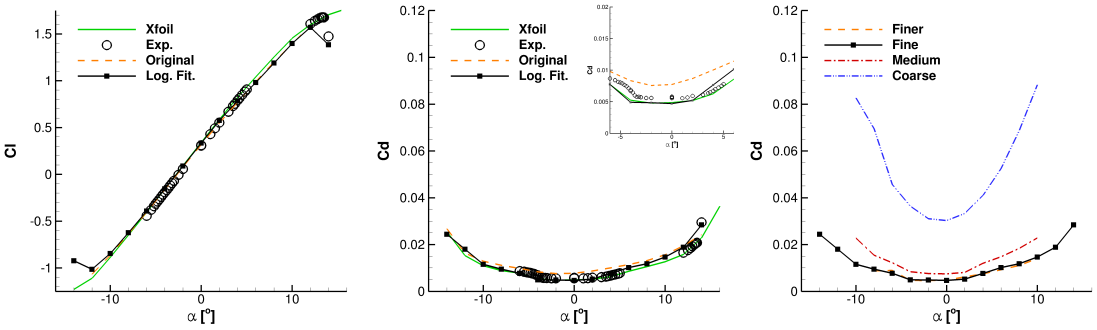

(a) Cl vs α. (b) Cd vs α. (c) Cd vs α.

Figure 7: Polars for DU00-w-212 aerofoil at $Re = 15 \times 10^6$, $Ma = 0.08$ and free-stream $Tu = 0.3346\%$ and $\mu_t/\mu = 5.0$.

	Xfoil	Log. Fit.	Original
low drag bucket extension	$(6°, -6°)$	$(6°, -8°)$	$(6°, -8°)$
$\alpha_{Cl=0}$	$-2.69°$	$-2.66°$	$-2.65°$
Cl_α	0.123	0.120	0.120

Table 3: Summary of the DU00-w-212 aerofoil design properties at $Re = 3 \times 10^6$, $Ma = 0.075$ and free-stream $Tu = 0.0864\%$ and $\mu_t/\mu = 0.05$.

	Xfoil	Log. Fit.	Original
low drag bucket extension	$(2°, -4°)$	$(2°, -4°)$	Failed to predict
$\alpha_{Cl=0}$	$-2.75°$	$-2.74°$	$-2.65°$
Cl_α	0.123	0.119	0.117

Table 4: Summary of the DU00-w-212 aerofoil design properties at $Re = 15 \times 10^6$, $Ma = 0.08$ and free-stream $Tu = 0.3346\%$ and $\mu_t/\mu = 5.0$.

4.2. 3-D Cases

Finally, the calibrated model has been employed to predict the flow around the AVATAR wind turbine blade presented in section 3 at three different wind speeds. In all cases, a free-stream $Tu = 0.0816\%$ and $\mu_t/\mu = 10.0$ have been used. For three-dimensional simulations there is no unique way to define the Reynolds number to be employed to evaluate the transition onset. However, since it is well known that for rotary wings the main contribution to the aerodynamic forces is generated in the region around the section at 75% radius; the local Reynolds number at this station, computed as

$$Re_{75\%R} = \frac{\rho_\infty \sqrt{{U_W}^2 + (0.75R \cdot \mathrm{RPM} \cdot \pi/30)^2} \cdot c_{\,75\%R}}{\mu} \tag{4}$$

has been employed to compute the C_{Onset1} employed in the simulations. For the test conditions with wind speeds 10.0, 10.5 and 12.0 considered here, the corresponding values of C_{onset1} were around 4.58, 4.65 and 4.74. Figure 8 confirms that the selected values at 75% blade radius represent reasonably well the value of C_{onset1} for a large part of the blade span where the main contributions to the aerodynamic forces are generated. Table 5 shows the predicted Power and Thrust produced by the wind turbine blade for the considered conditions. As expected, when laminar to turbulent transition is considered an increase of power and thrust of about $15 - 20\%$ and $8 - 10\%$, respectively, is obtained with respect to fully-turbulent results. Moreover, when fully-turbulent flow is considered a decrease in the performance of the blade is observed at wind speed higher than the design point of $U_W = 10.5m/s$. Contours of C_f on the suction and pressure side of the blade are presented in figures 9a and 9b. The transition position is around half of the chord in the region around 75% radius on both pressure and suction sides. However, towards the blade root the transition position moves towards the LE on the suction side and the TE on the pressure side as result of the effect of the lower rotational speed on the local angle of attack.

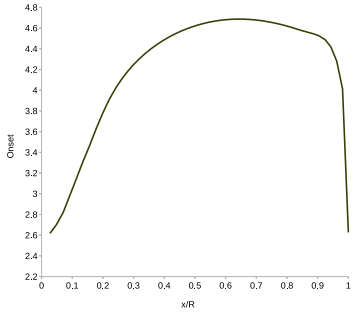

Figure 8: C_{onset1} values along the blade where the local Reynolds number is evaluated using equation (4) for the $U_W = 10.5$m/s test case.

	Fully-Turbulent Flow			Transitional Flow		
U_W (m/s)	10.0	10.5	12.0	10.0	10.5	12.0
Power (KW)	8150.97	9469.98	9038.53	9432.87	10925.75	10837.78
Thrust (KN)	1228.55	1357.60	1048.42	1331.98	1473.83	1155.48

Table 5: Power and Thrust as function of the wind speed for the AVATAR wind turbine blade.

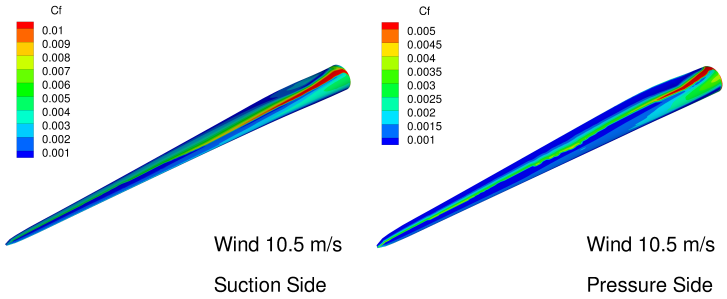

(a) . (b) .

Figure 9: Skin friction coefficient contours for the suction and pressure sides of the AVATAR wind turbine blade at different wind conditions.

5. Conclusions and Future Work

The LCTM concept was introduced by Menter et. al. [9] almost a decade ago to include transitional flows modeling in general-purpose CFD codes. This due to the fact that the commonly employed e^N method requires a complex infrastructure that limit its applicability in complex CFD simulations. Recently, a simplified version of model has been presented [11] reducing the formulation to only the γ-equation providing tunable coefficients to match the required application. The model has been assessed for various test cases however, further works are needed to evaluate the γ-equation model at more extreme conditions such as high Reynolds numbers (i.e. $Re \geq 1 \times 10^6$), very low Reynolds numbers (i.e. $Re \leq 50 \times 10^3$) and supersonic/hypersonic flows.

In this paper the, $\gamma-$equation transition model is calibrated for all Reynolds numbers flows, at low Mach numbers, to be employed in wind turbine applications. The calibration process consisted in a rescaling of C_{TU1} and C_{TU2} in equation (2) from 100.0 and 1000.0 to 163.0 and 1002.25, respectively, and a logarithmic curve has been proposed to define the transition onset, C_{Onset1}, as a function of the Reynolds number for $1 \times 10^6 \leq Re \geq 15 \times 10^6$. The proposed improvements to the model shown promising results for both two-dimensional and three-dimensional flows, even if cross-flow instabilities are neglected and only natural transition, i.e. $Tu < 1\%$, has been considered. Compared to the original model at high Reynolds numbers, while the latter displays a decay of the accuracy, the proposed calibrated model maintains a good level of reliability and retains the accuracy of the original model at lower Re. This shows that the original model can be improved and in future works further transitional effects such as cross-flow instabilities and high-Mach effect could be included.

Acknowledgments

Results were obtained using the EPSRC founded ARCHIE-WeSt HPC (www.archie-west.ac.uk). EPSRC grant no. EP/K000586/1. Simone Colonia is supported by the AVATAR project (FP7-ENERGY-2013-1/N608396). Vladimir Leble is supported by the MARE-WINT project (FP7-PEOPLE-2012-ITN/309395).

References

[1] Aupoix B, Arnal D, Bezard H, Chaouat B, Chedevergne F, Deck S, Gleize V, Grenard P and Laroche E 2011 *Aerospace Lab Journal* **2**
[2] Smith A and Gamberoni N 1956 *Report No. ES 26388 - Douglas Aircraft Co.*
[3] van Ingen J 1956 *Report No UTH-74 - Delft University of Technology*
[4] Archambaud J P, Arnal D, Sraudie A, Carrier G and Louis F 2005 *CEAS Katnet Conference on Key Aerodynamic Technologies*
[5] Krumbein A 2008 *Aerospace Science and Technology* **12** 592598
[6] Abu-Ghannam B and Shaw R 1980 *Journal of Mechanical Engineering Science* **22** 213–228
[7] Michel R 1951 *Technical Report 1/1578A - ONERA*
[8] Cebeci T and Smith A 1974 *Analysis of Turbulent Boundary Layers* (Academic Press, New York)
[9] Menter F, Langtry R and Völker S 2006 *Flow Turbulence and Combustion* **77** 277–303
[10] Langtry R and Menter F 2009 *AIAA Journal* **47** 2894–2906
[11] Menter F, Smirnov PE Tao L and Avancha R 2015 *Flow Turbulence and Combustion* **95** 583–619
[12] Snel H 1998 *Wind Energy* **1** 46–69
[13] Brodeur R and van Dam C 2001 *Wind Energy* **4** 61–75
[14] Sørensen N 2009 *Wind Energy* **12** 715–733
[15] Khayatzadeh P and Nadarajah S 2014 *Wind Energy* **17** 901–918
[16] Lawson S J, Steijl R, Woodgate M and Barakos G 2012 *Progress in Aerospace Science* **52** 19–29
[17] Barakos G, Steijl R, Badcock K and Brocklehurst A 2005 *31st European Rotorcraft Forum* pp Paper No. 91, 19–29
[18] Menter F 1994 *AIAA Journal* **32** 1598–1605
[19] Kato M and Launder B 1993 *9th Symposium on Turbulent Shear Flows*
[20] Spalart P and Rumsey C 2007 *AIAA Journal* **45** 2544–2553
[21] AVATAR project *www.eera-avatar.eu* accessed 08/2016
[22] Barakos G and Gomez-Iradi S 2008 *Proceedings of the Institution of Mechanical Engineers Part A: Journal of Power and Energy* **222** 455–470
[23] Gomez-Iradi S, Steijl R and Barakos G 2009 *Journal of Solar Energy Engineering* **131** 031009
[24] Carrión M, Woodgate M, Steijl R, Barakos G, Munduate X and Gomez-Iradi S 2015 *Wind Energy* **18** 10231045
[25] Carrión M, Woodgate M, Steijl R, Barakos G, Gomez-Iradi S and Munduate X 2015 *AIAA Journal* **3** 588–602
[26] Drela M and Giles M 1987 *AIAA Journal* **25** 1347–1355
[27] Energy research Centre of the Netherlands (Energieonderzoek Centrum Nederland) *www.ecn.nl* accessed 08/2016
[28] National Renewable Energy Centre of Spain (Centro Nacional de Energas Renovable) *www.cener.com* accessed 08/2016